THE JOURNAL OF BIOLOGICAL CHEMISTRY VOL. 288, NO. 27, pp. 19471–19483, July 5, 2013

Conserved Gating Elements in TRPC4 and TRPC5 Channels*

Received for publication, April 17, 2013, and in revised form, May 15, 2013 Published, JBC Papers in Press, May 15, 2013, DOI 10.1074/jbc.M113.478305

Andreas Beck[‡1,2], Tilman Speicher[‡1], Christof Stoerger[‡], Thomas Sell[‡], Viviane Dettmer[‡], Siti A. Jusoh[§¶], Ammar Abdulmughni[§], Adolfo Cavalié[‡], Stephan E. Philipp[‡], Michael X. Zhu[‖], Volkhard Helms[§], Ulrich Wissenbach[‡], and Veit Flockerzi[‡]

From the [‡]Experimentelle und Klinische Pharmakologie und Toxikologie, Universität des Saarlandes, 66421 Homburg, Germany, the [§]Zentrum für Bioinformatik, Universität des Saarlandes, 66123 Saarbrücken, Germany, the [¶]Faculty of Pharmacy, Universiti Teknologi MARA, 42300 Bandar Puncak Alam, Malaysia, and the [‖]Department of Integrative Biology and Pharmacology, University of Texas Health Science Center at Houston, Houston, Texas 77030

Background: Gating mechanisms of TRPC channels are mostly unknown.
Results: Replacing the highly conserved glycine residue within the linker between transmembrane domains 4 and 5 by serine renders TRPC4 and TRPC5 channels constitutively active.
Conclusion: TRPC channel opening seems to require similar constraints than the voltage-gated potassium channels.
Significance: Novel mechanistic insights into structural requirements of TRPC channel gating are provided.

TRPC4 and TRPC5 proteins share 65% amino acid sequence identity and form Ca^{2+}-permeable nonselective cation channels. They are activated by stimulation of receptors coupled to the phosphoinositide signaling cascade. Replacing a conserved glycine residue within the cytosolic S4–S5 linker of both proteins by a serine residue forces the channels into an open conformation. Expression of the $TRPC4_{G503S}$ and $TRPC5_{G504S}$ mutants causes cell death, which could be prevented by buffering the Ca^{2+} of the culture medium. Current-voltage relationships of the $TRPC4_{G503S}$ and $TRPC5_{G504S}$ mutant ion channels resemble that of fully activated TRPC4 and TRPC5 wild-type channels, respectively. Modeling the structure of the transmembrane domains and the pore region (S4-S6) of TRPC4 predicts a conserved serine residue within the C-terminal sequence of the predicted S6 helix as a potential interaction site. Introduction of a second mutation (S623A) into $TRPC4_{G503S}$ suppressed the constitutive activation and partially rescued its function. These results indicate that the S4–S5 linker is a critical constituent of TRPC4/C5 channel gating and that disturbance of its sequence allows channel opening independent of any sensor domain.

TRPC[3] channels are *in vivo* coincidence detectors, which integrate multiple signal transduction pathways originating from the plasma membrane (1, 2). They provide specific transmembrane signaling pathways, shape the membrane potential, and accomplish Ca^{2+} entry. Thereby, they essentially trigger a variety of functions in excitable and nonexcitable cells. Seven mammalian TRPC proteins (TRPC1–7) have been identified that can be divided into three subgroups by amino acid sequence similarity, C1/C4/C5 (41% sequence identity), C3/C6/C7 (69% sequence identity), and C2. The TRPC proteins form tetrameric channels, which are activated after stimulation of G-protein-coupled receptors or receptor tyrosine kinases linked to phospholipase Cβ or -γ, respectively.

The mammalian TRPC4 and TRPC5 proteins share 65% sequence identity and were initially identified by their sequence similarity with the *Drosophila* TRP protein (~40% sequence identity), the founding member of the TRP superfamily of proteins. TRPC4 is expressed in a broad range of tissues, including brain, endothelium, and intestinal smooth muscle. In smooth muscle cells, TRPC4 channels are gated by muscarinic acetylcholine receptors and contribute more than 80% to the muscarinic receptor-induced cation current (mI_{CAT}) (3). In these cells, TRPC4 channels couple muscarinic receptors to smooth muscle cell depolarization, voltage-activated Ca^{2+} influx, and contraction, and thereby accelerate small intestinal motility (3). TRPC5 is predominantly expressed in the brain (4). Although channel properties are similar to those of TRPC4, TRPC5 channels are cold-sensitive (5) and can be activated by a variety of additional stimuli, including a rise of cytosolic Ca^{2+} (6).

The predicted transmembrane topology indicates that TRPC proteins structurally resemble voltage-gated K^+ channel proteins, and the overall architecture of TRPC channels and voltage-gated K^+ channels is presumably similar. However, their structural relation is not close enough to build functional hybrid channels (7). Nevertheless, like the voltage-gated K^+ channel proteins, the TRPC proteins encompass six putative transmembrane helices (S1–S6) (8). Their S1–S4 segments form the sensor domain, and upon tetramerization their S5 and S6 segments constitute a central ion-conducting pore (8). In voltage-gated K^+ channels, the cytosolic S4–S5 linker connects the S1–S4 helices to the S5–S6 pore. It triggers motion of the S6 helices to open or close the pore in response to voltage changes. These voltage changes are detected by a typical voltage sensor domain in S4 consisting of four negatively charged amino acid

* This work was supported by Deutsche Forschungsgemeinschaft Grant SFB894 (to A. B., S. E. P., and V. F.), the Homburg Forschungsförderungsprogramm HOMFOR (to A. B., C. S., and S. E. P.), and the Forschungskommission der Universität des Saarlandes (to A. B., S. E. P., U. W., and V. F.).
[1] Both authors contributed equally to this work.
[2] To whom correspondence should be addressed. Fax: 49-6841 1626402; E-mail: andreas.beck@uniklinikum-saarland.de.
[3] The abbreviations used are: TRPC, transient receptor potential canonical; TRP, transient receptor potential; IRES, internal ribosomal entry site; NMDG, *N*-methyl-D-glucamine; M_2R, muscarinic acetylcholine receptor type 2; CCh, carbachol; TM, transmembrane.

residues (9, 10). Along these lines, a state-dependent interaction between the S4–S5 linker and a site in the S6 transmembrane segment has been suggested to stabilize the closed state of the depolarization-activated Kv7.1 (KCNQ1) channel (11, 12) and the open state of hyperpolarization-activated potassium channels like KAT1 (13) and HCN (14). Although TRP channels lack the typical voltage sensor domain of voltage-activated K^+ channels in transmembrane segment S4, the opening of TRPC4 and TRPC5 channels may require similar structural constraints. We identified a conserved glycine residue within the S4–S5 linkers of TRPC4 and TRPC5 being crucial in this respect. Mutation of this glycine in either channel protein to a serine keeps the channels in a constitutive open conformation. This "gain-of-function" mutation was partially rescued by introducing a second mutation just C-terminal of the predicted S6 helix. Our data indicate that the glycine residues at position 503 and 504 identified in the S4–S5 linker of TRPC4 and TRPC5, respectively, are crucial for keeping the channels in a closed and gateable conformation.

EXPERIMENTAL PROCEDURES

Cells, Transfected cDNA, and Transfection—HEK-293 cells (ATCC, CRL 1573) were obtained from the American Type Culture Collection (ATCC, Manassas, VA); the Flp-In™-293 cells were from Invitrogen. HEK-293 cell lines stably expressing the muscarinic acetylcholine receptor type 2 (M_2R), TRPC4 (or both) and TRPC5, respectively, were described previously (15). HEK-293 cells and/or HEK-293 M_2R cells were transiently transfected with 3 μg of cDNA (TRPC4, $TRPC4_{G503S}$, $TRPC4_{G503A}$, $TRPC4_{G503M}$, $TRPC4_{G503L}$, $TRPC4_{G503S/S623A}$, $TRPC5_{G504S}$, and $TRPC5_{G504C}$) in 5 μl of the PolyFect® reagents (Qiagen, Hilden, Germany). To obtain the bicistronic expression plasmids pdiTRPC4 and pdiTRPC5, the entire coding regions of mouse TRPC4 (accession number NM_016984.3) and mouse TRPC5 (accession number NM_009428.2) were subcloned into the pCAGGS-IRES-GFP vector downstream of the chicken β-actin promotor followed by the consensus sequence for initiation of translation in vertebrates; the stop codons are followed by an IRES and the green fluorescent protein (GFP) cDNA. To generate stable inducible Flp-In™ cell lines, the $TRPC4_{G503S}$ and the $TRPC5_{G504S}$ cDNAs were subcloned into the pcDNA5/FRT/TO vector. For patch clamping and Ca^{2+} imaging, wild-type or stably M_2R-expressing HEK-293 cells were plated on glass coverslips 24 h after transfection, and experiments were performed at indicated times. HEK-293 cells stably expressing TRPC4 (with and without the M_2 receptor) and TRPC5 and Flp-In™-293 cells expressing $TRPC4_{G503S}$ or $TRPC5_{G504S}$ after induction in the presence of tetracycline (10 μg/ml) were grown on glass coverslips and were used up to 48 h after plating or induction. All cells, except after transient transfection of $TRPC5_{G504S}$ (see below), were grown in minimal essential medium containing 10% fetal calf serum.

Site-directed Mutagenesis—Mutagenesis was carried out using the QuikChange™ site-directed mutagenesis kit (Stratagene, La Jolla, CA) as described previously. To generate the point mutations, the TRPC4, TRPC5, and $TRPC4_{G503S}$ cDNAs in pBluescriptSK− (Stratagene) were used as templates and the following primer pairs for PCR: $TRPC4_{G503S}$, 5′-GCC AAT TCT CAC CTG TCG CCT CTG CAG ATA TC-3′ and 5′-GAT ATC TGC AGA GGC GAC AGG TGA GAA TTG GC-3′; $TRPC5_{G504S}$, 5′-AGC CCT CTG CAG ATC TCT TTG G-3′ and 5′-TAA ATG GGA GTT GGC TGT GAA C-3′; $TRPC5_{G504C}$, 5′-TGC CCT CTG CAG ATC TCT TTG G-3′ and 5′-TAA ATG GGA GTT GGC TGT GAA C-3′; $TRPC4_{G503S/S623A}$, 5′-ATT ATT CAT CAT AGC AAT T-3′ and 5′-GCA TAC CAA CTA ATT GCC GAC CAT G-3′; $TRPC4_{G503A}$, 5′-GCT CCT CTG CAG ATA TCT CTG GG-3′ and 5′-CAG GTG AGA ATT GGC AGT G-3′; $TRPC4_{G503L}$, 5′-CTG CCT CTG CAG ATA TCT CTG GG-3′ and 5′-CAG GTG AGA ATT GGC AGT G-3′; and $TRPC4_{G503M}$, 5′-ATG CCT CTG CAG ATA TCT CTG GG-3′ and 5′-CAG GTG AGA ATT GGC AGT G-3′. Amplified cDNAs were subcloned into the pCAGGS-IRES-GFP vector ($TRPC4_{G503S}$, $TRPC4_{G503A}$, $TRPC4_{G503M}$, $TRPC4_{G503L}$, $TRPC4_{G503S/S623A}$, $TRPC5_{G504S}$, and $TRPC5_{G504C}$), and the pcDNA5/FRT/TO vector ($TRPC4_{G503S}$ and $TRPC5_{G504S}$). All mutant cDNAs were sequenced on both strands.

Cell Viability Assays—HEK-293 cells grown on coverslips (2.5 cm) were transfected with $TRPC5_{G504S}$-IRES-GFP cDNA and cultured in minimal essential medium containing 10% fetal calf serum in the absence and presence of 1.3, 1.7, 1.9, 2.1, 2.3, and 2.5 mM EGTA buffering the free Ca^{2+} concentration (~2 mM in total) in the culture medium to 700, 301, 103, 3.2, 1, and 0.7 μM, respectively (calculated with WebMaxC). The number of green fluorescent cells in 10 randomly chosen fields of view (×10 magnification) were counted, averaged, and plotted *versus* the concentration of free Ca^{2+} in the culture media. To assess viability, Flp-In™-293 cells expressing $TRPC4_{G503S}$ or $TRPC5_{G504S}$ and HEK-293 cells transiently expressing the $TRPC4_{G503S/S623A}$-IRES-GFP cDNA were grown in cell culture flasks in minimal essential medium containing 10% fetal calf serum (with Ca^{2+}) and split into 96-well plates. The cells were counted using a flow cytometer (Guava EasyCyte 8HT) at indicated time points after induction/transfection, and the percentage of living cells, detected as viable by the incubation with Guava ViaCount reagent, was plotted *versus* time. To evaluate the effect of the TRPC channel inhibitor SKF 96365 on viability, the cells were grown for 48 h in the presence of the indicated concentrations of SKF 96365 in the culture media and then counted by the cytometer as above.

Western Blot Analysis—Lysates were prepared from HEK-293 wild-type cells and the various TRPC4- and TRPC5-expressing HEK-293 and Flp-In™-293 cells. Cells were grown up to 80–90% confluence on 3.5-cm dishes. After removing the medium and washing in the presence of PBS, the cells were lysed in the presence of 150 μl of Laemmli buffer. The proteins of the lysate were denatured and subjected to 8% SDS-PAGE. Proteins were transferred onto a nitrocellulose membrane and probed with antibodies for TRPC4 and TRPC5 (in-house generated affinity-purified antibodies 1056 (mTRPC4) and 3B3-A5 (mTRPC5)). Proteins were detected using horseradish peroxidase-coupled secondary antibodies and the Western Lightning chemiluminescence reagent Plus (PerkinElmer Life Sciences). Original scans were saved as TIFF files from LAS 3000 (Fujifilm), which were further processed in Adobe Photoshop

and/or CorelDraw. Images were cropped, resized proportionally, and brought to the resolution required for publication.

Cell Surface Biotinylation—Nontransfected HEK-293 cells and cells transiently expressing $TRPC4_{G503S/S623A}$ grown up to 80–90% confluency in 3.5-cm culture dishes were placed on ice and washed twice with ice-cold phosphate-buffered saline (PBS, pH 8) supplemented with 1 mM $MgCl_2$ and 0.5 mM $CaCl_2$. After incubation in the presence of sulfosuccinimidyl-6-(biotinamido) hexanoate (0.5 mg/ml) at 4 °C for 30 min, the dishes were rinsed twice with PBS supplemented with 1 mM $MgCl_2$, 0.5 mM $CaCl_2$, and 0.1% bovine serum albumin and once with PBS, pH 7.4. Cells were harvested in the presence of PBS supplemented with 2 mM EGTA, centrifuged at 1000 × *g* at 4 °C for 5 min, resuspended in ice-cold PBS, pH 7.4, supplemented with 1% Triton X-100, 1 mM EDTA, and a mixture of protease inhibitors (lysis buffer), and incubated for 30 min at 4 °C. Cellular debris was removed by centrifugation at 1000 × *g* and 4 °C for 5 min. Samples containing 600 μg of protein were incubated in the presence of avidin-agarose beads (150 μl of suspension, pre-equilibrated in lysis buffer) at 4 °C for 3 h. After centrifugation (1000 × *g*) at 4 °C for 5 min, the precipitated beads were washed four times with lysis buffer supplemented with NaCl to give a final concentration of 0.4 M NaCl. Proteins were eluted by 2× Laemmli buffer (60 μl), denatured (37 °C for 30 min), separated by SDS-PAGE, and thereafter blotted on nitrocellulose membranes.

Homology Modeling—Primary sequences of the TRP proteins were retrieved from the Uniprot database. As template for homology modeling, we used the crystal structure 3LUT of the Kv1.2 channel that was obtained from the Protein Data Bank. Initially, the putative transmembrane domains of each TRP channel were predicted with the TOPCONS server that combines predictions from five different topology algorithms (16). Then the sequences representing the consensus region of the transmembrane domain were used as input for a multiple sequence alignment between the target proteins and the 3LUT template (17) using the program ClustalW2 (18). The program Jalview (19) was used to visually inspect the final alignment and to convert the MSA to pir format. Finally, three-dimensional models were built by the Modeler9 package (20). For each TRP sequence, 15 models were computed. Subsequently, the best model (with the highest discrete optimized protein energy score) was selected for further refinement with Modeler using default scripts.

Electrophysiological Recordings and Solutions—Membrane currents were recorded in the tight seal whole-cell patch clamp configuration using an EPC-9 amplifier (HEKA Electronics, Lambrecht, Germany). Patch pipettes were pulled from glass capillaries GB150T-8P (Science Products, Hofheim, Germany) at a vertical Puller (PC-10; Narishige, Tokyo, Japan) and had resistances between 2 and 4 megaohms when filled with standard internal solution (in mM: 120 cesium glutamate, 8 NaCl, 1 $MgCl_2$, 10 HEPES, 10 1,2-bis(2-aminophenoxy)ethane-*N*,*N*,*N*′,*N*′-tetraacetic acid tetracesium salt, 3.1 $CaCl_2$ (100 nM free Ca^{2+}, calculated with WebMaxC), pH adjusted to 7.2 with CsOH). Instead of 3.1 mM $CaCl_2$, 0 or 9.8 mM was added to obtain 0 and 10 μM free Ca^{2+}, respectively. Standard external solution contained the following (in mM): 140 NaCl, 2 $MgCl_2$, 1 $CaCl_2$, 10 HEPES, 10 glucose, pH adjusted to 7.2 with NaOH. For monovalent cation-free solution Na^+ was replaced by NMDG. IsoCa (0Na) solution contained (in mM) 125 $CaCl_2$, 10 HEPES, and 10 glucose, pH adjusted to 7.2 with NMDG, and isoNa (0Ca) solution contained (in mM) 140 NaCl, 3 $MgCl_2$, 10 HEPES, and 10 glucose, pH adjusted to 7.2 with NaOH. The La^{3+} application contained 2 or 0.1 mM $LaCl_3$, and for M_2 receptor stimulation 100 μM carbachol were added to the respective external solution. Osmolarity of all solutions ranged between 285 and 315 mOsm.

Voltage ramps of 400 ms duration spanning a voltage range from −100 to 100 mV were applied at 0.5 Hz from a holding potential of 0 mV over a period of 150–500 s using the PatchMaster software (HEKA). All voltages were corrected for a 10-mV liquid junction potential. Currents were filtered at 2.9 kHz and digitized at 100-μs intervals. Capacitive currents and series resistance were determined and corrected before each voltage ramp using the automatic capacitance compensation of the EPC-9. Inward and outward currents were extracted from each individual ramp current recording by measuring the current amplitudes at −80 and 80 mV, respectively, and plotted *versus* time. Current-voltage (IV) relationships were extracted at indicated time points. For some experiments, the inward and outward currents were normalized to the cell capacitance to get the current density in picoampere/picofarad.

Ca^{2+} Imaging—Intracellular live cell Ca^{2+} imaging experiments were performed using a Polychrome V and CCD camera (ANDOR iXon 885, ANDOR Technology, South Windsor, CT)-based imaging system from TILL Photonics (Martinsried, Germany) at a Zeiss Axiovert 200M fluorescence microscope equipped with a ×20 Zeiss Plan Neofluar objective. Data acquisition was accomplished with the imaging software TILLVision (TILL Photonics). Prior to the experiments, cells were incubated in media supplemented with 5 μM of the Ca^{2+}-sensitive fluorescent dye fura-2-AM for 30 min in the dark at room temperature and washed twice with nominally Ca^{2+}-free external solution (in mM: 140 NaCl, 5 KCl, 1 $MgCl_2$, 10 HEPES, 10 glucose, pH adjusted to 7.2 with NaOH) to remove excess fura-2-AM. The fura-2-loaded cells, growing on 2.5-cm glass coverslips, were transferred to a bath chamber containing nominally Ca^{2+}-free solution, and fura-2 fluorescence emission was monitored at >510 nm after excitation at 340 and 380 nm for 30 ms each at a rate of 1 Hz for 600 s. Cells were marked, and the ratios of the background-corrected fura-2 fluorescence at 340 and 380 nm (F_{340}/F_{380}) were plotted *versus* time.

Data Analysis—Initial whole-cell patch clamp and Ca^{2+} imaging analyses were performed with FitMaster (HEKA) and TILLVision (TILL Photonics), respectively. IGOR Pro (Wave Metrics, Lake Oswego, OR) was used for further analysis and for preparing the figures. Where applicable, the data were averaged and given as means ± S.E. for a number (n) of cells. For Ca^{2+} imaging data, the number of averaged experiments (x) and the number of included cells (n) are given as (x/n).

Relative Ca^{2+} permeabilities (P_{Ca}/P_{Na}) of TRPC4 wild-type and mutant channels were calculated using Equation 1,

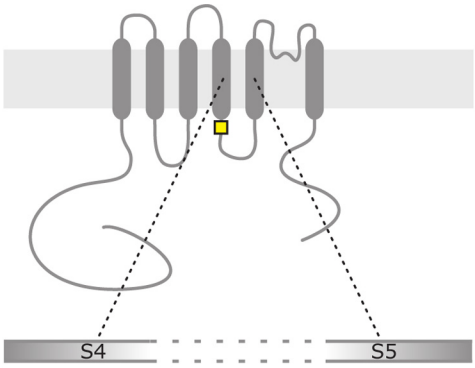


```
Yvc1     YLESQRFIGIMLVILK-HMMKESIVFFFLL
dTRP     IFSINPHLGPLQVSLG-RMIIDIIKFFFIY
TRPV4    FTRGLKLTGTYSIMIQKILFKDLFRFLLVY
TRPV3    YTRGFQSMGMYSVMIQKVILHDVLKFLFVY
TRPC3    ILPANESFGPLQISLG-RTVKDIFKFMVLF
TRPC4    LFTANSHLGPLQISLG-RMLLDILKFLFIY
TRPC5    LFTANSHLGPLQISLG-RMLLDILKFLFIY
```

FIGURE 1. **Alignment of the cytosolic S4–S5 linker in TRP proteins.** Transmembrane topology of a TRP channel protein with transmembrane helices S1 to S6, intracellular N and C termini, and alignment of the amino acid sequences of the cytosolic S4–S5 linker of yeast Yvc1 (accession number NP_014730), *Drosophila* (*d*)TRP (NP_476768.1), human TRPV4 (NP_067638.3), and mouse TRPV3 (NP_659567), TRPC3 (NP_062383), TRPC4 (NM_016984.3), and TRPC5 (NM_009428.2) are shown. The published sites of mutations leading to constitutive channel activity (*red*) and the conserved glycine residues (*yellow*) are indicated. Alignment was obtained by the *MUSCLE* and prediction of transmembrane helices by the *TMHMM* algorithms.

$$\frac{P_{Ca}}{P_{Na}} = \frac{[Na]_o \times e^{\frac{F \times (V_{Ca} - V_{Na})}{R \times T}} \times (1 + e^{\frac{F \times V_{Ca}}{R \times T}})}{4 \times [Ca]_o} \qquad \text{(Eq. 1)}$$

with $R = 8.314$ J/(mol·K), $T = 297$ K, and $F = 96485$ C/mol (21). V_{Ca} and V_{Na} represent the reversal potentials of the currents in external saline containing just Ca^{2+} ($[Ca]_o$) or just Na^+ ($[Na]_o$), respectively (see Fig. 7).

Chemicals—Fura-2-AM was purchased from Molecular Probes (Eugene, OR), all other chemicals were from Sigma.

RESULTS

S4–S5 Linker Alignment—Several gain-of-function mutations within the S4–S5 linker of TRP genes have been identified, including the yeast Yvc1 F380L (22), the *Drosophila* TRP F550I (23), the human TRPV4 R594H, R616Q, and V620I (24, 25), the human, mouse, and rat TRPV3 G573S, and G573C (26–29), and the mouse TRPC3 T635A mutations (30), which are indicated in *red* in Fig. 1. The alignment of the S4–S5 linker sequences of these different TRP proteins with the corresponding sequences of TRPC4 and TRPC5 reveals that none of the amino acid residues affected by those mutations are conserved except the glycine residue at position 573 of the human, rat, and mouse TRPV3, which corresponds to position 503 and 504 of the mouse TRPC4 and TRPC5, respectively (Fig. 1, *yellow box*). In TRPV3, the spontaneous G573S or G573C mutations have been associated with the *Nh (non-hair)* and *Ht (hypotrichosis)* mutations in rodents, which are associated with defective hair growth and dermatitis (28), and the Olmsted syndrome in human, which is associated with palmoplantar and periorificial keratoderma and severe itching (26, 27). Introducing these mutations in the mouse or human TRPV3 cDNA results in constitutively active channels in the heterologous HEK-293 expression system (26, 29).

Cell Survival Is Affected by G503S and G504S Mutation in TRPC4 and TRPC5, Respectively—By site-directed mutagenesis, we replaced the conserved glycine residue in the S4–S5 linker in TRPC5 by a serine or a cysteine residue. In a first series of experiments, we transiently expressed the $TRPC5_{G504S}$ or $TRPC5_{G504C}$ cDNA in HEK-293 cells, and we noticed that in both populations a considerable fraction of cells did not survive. Most probably the introduced mutations render the channels open thereby allowing nonrestricted Ca^{2+} influx into the transfected cells, which causes cell death. Therefore, in a second series of experiments, cells transfected with the $TRPC5_{G504S}$ cDNA were continuously grown in the presence of increasing concentrations of EGTA in the culture medium reducing its free Ca^{2+} concentration to less than 1 μM. Under these conditions, a substantial number of transfected cells survived (Fig. 2*A*). To measure Ca^{2+} influx, we kept the cells in nominally Ca^{2+}-free solution, added 2.5 mM Ca^{2+} to the bath solution, and monitored changes of the cytosolic Ca^{2+} concentration. As shown in Fig. 2*B*, Ca^{2+} influx (F_{340}/F_{380}) increased with time after transfection in $TRPC5_{G504S}$-expressing cells independent of any receptor activation. Next, we generated two cell lines with tetracycline-inducible $TRPC5_{G504S}$ and $TRPC4_{G503S}$ cDNAs. After induction, the $TRPC5_{G504S}$ and the $TRPC4_{G503S}$ proteins are expressed (Fig. 2, *C* and *F*). We next measured cell survival when growing the cells in the presence of "normal" Ca^{2+} (2 mM) in the culture medium. As shown in Fig. 2, *D* and *G*, the number of viable $TRPC5_{G504S}$- and $TRPC4_{G503S}$-expressing cells declined over time to about 40% within 48 h after induction, although we could not detect any changes in the survival rate of noninduced cells. Growing the induced $TRPC5_{G504S}$- and $TRPC4_{G503S}$-expressing cells for 48 h in the presence of different concentrations of SKF 96365 attenuates the rate of cell death in the range of 100 μM, a concentration known to block TRP channel activity (Fig. 2, *E* and *H*). However, higher concentrations of SKF 96365 resulted in a massive reduction of living cells even in the noninduced culture.

Taken together, these data suggest that after induction of $TRPC4_{G503S}$ and $TRPC5_{G504S}$ expression, constitutive Ca^{2+} influx takes place leading to cell death because of Ca^{2+} overload. To measure Ca^{2+} influx in the inducible cell lines, we monitored Ca^{2+} influx either without induction ("0 h") or with induction of $TRPC5_{G504S}$ and $TRPC4_{G503S}$ expression for 5 or 18–20 h (Fig. 2, *I* and *J*). As controls, we used cell lines stably expressing wild-type TRPC4 or TRPC5 proteins ($TRPC4_{WT}$ and $TRPC5_{WT}$). Compared with noninduced cells, the wild-type controls show, at best, only a small increase of cytosolic Ca^{2+} in response to re-addition of extracellular Ca^{2+}. In contrast, cells expressing the $TRPC5_{G504S}$ and $TRPC4_{G503S}$ mutants after induction reveal a substantial Ca^{2+} influx, which increased over time (Fig. 2, *I* and *J*).

Functional Characterization of Mutant TRPC Channels—Next, we measured the ionic currents after induction of $TRPC4_{G503S}$ expression. Like the Ca^{2+} influx, constitutive current activities were detected upon establishing the whole-cell configuration, and the current amplitudes, measured at −80 and 80 mV, increased with time after induction (Fig. 3*A*). Fig.

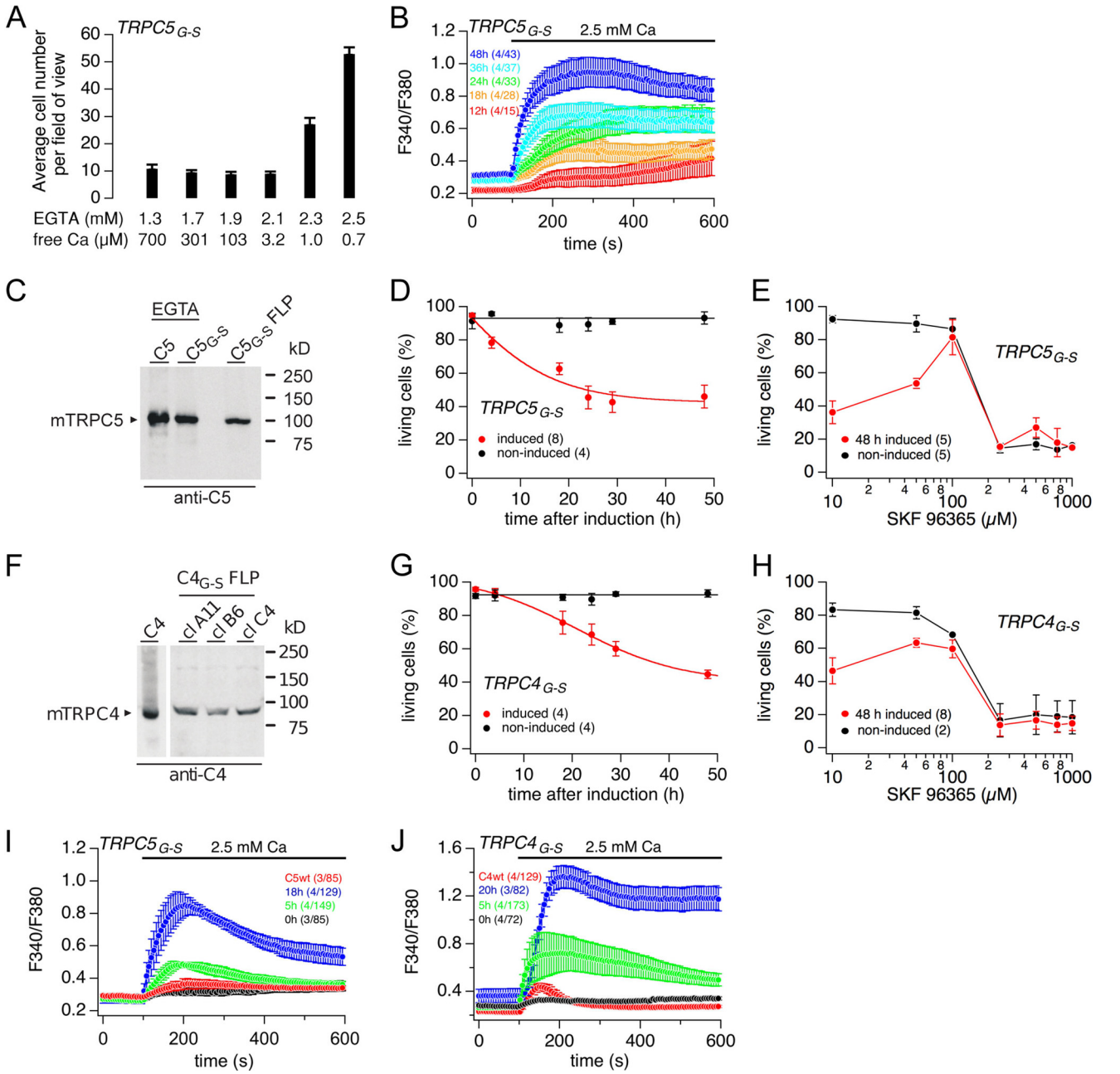

FIGURE 2. **Spontaneous Ca^{2+} influx in $TRPC5_{G\text{-}S}$- and $TRPC4_{G\text{-}S}$-expressing cells.** *A*, HEK-293 cells were transfected with $TRPC5_{G\text{-}S}$-IRES-GFP cDNA and kept for 48 h in media containing 1.3–2.5 mM EGTA (700 to 0.7 μM free Ca^{2+}). The green (transfected) cells from 10 randomly chosen fields of view (×10 magnification) were counted, averaged, and plotted *versus* EGTA (free Ca^{2+}) concentration in the media. *B*, cells transfected with $TRPC5_{G\text{-}S}$-IRES-GFP cDNA were grown in the presence of 2.5 mM EGTA for 12–48 h after transfection. Imaging experiments started in nominally Ca^{2+}-free solution, and cytosolic Ca^{2+} concentration, represented by the fura-2 fluorescence ratio (F_{340}/F_{380}), was measured *versus* time. Ca^{2+} influx was challenged by adding 2.5 mM Ca^{2+} to the bath solution. *C* and *F*, Western blot. Expression of TRPC5 (*C5*) and $TRPC5_{G504S}$ ($C5_{G\text{-}S}$) (*C*) and TRPC4 (*C4*) in HEK-293 (*F*), and $TRPC5_{G504S}$ ($C5_{G\text{-}S}$) (*C*) and $TRPC4_{G503S}$ ($C4_{G\text{-}S}$) in Flp-In™-293 cells (*FLP*) 16 h after induction (*F*); $C4_{G\text{-}S}$ FLP cell clone A11 was used for experiments. HEK-293 cells expressing TRPC5 and $TRPC5_{G\text{-}S}$ were grown in the presence of 2.5 mM EGTA (*C*). *D*, *E*, *G*, and *H*, viability assays of HEK-293 cells inducibly expressing $TRPC5_{G\text{-}S}$ (*D* and *E*) and $TRPC4_{G\text{-}S}$ (*G* and *H*). *D* and *G*, cells were induced (or noninduced as control) and grown for 0–48 h (as indicated). The percentage of living cells, counted by a flow cytometer (Guava EasyCyte 8HT), was plotted *versus* time after induction. *E* and *H*, viability of HEK-293 cells expressing $TRPC5_{G\text{-}S}$ (*E*) or $TRPC4_{G\text{-}S}$ (*H*), grown in different concentrations of the nonspecific TRPC channel inhibitor SKF 96365. The percentage of living cells was plotted *versus* the concentration of SKF 96365 in the culture medium 48 h after induction (control = no induction). *I* and *J*, HEK-293 cells inducibly expressing $TRPC5_{G\text{-}S}$ (*I*; 0, 5, and 18 h after induction) and $TRPC4_{G\text{-}S}$ (*J*; 0, 5, and 20 h after induction) or stably expressing the corresponding wild-type ($C4_{WT}$ and $C5_{WT}$) were loaded with fura-2-AM and kept in nominally Ca^{2+}-free bath solution. Ca^{2+} influx was challenged by adding 2.5 mM Ca^{2+} to the bath solution, and the cytosolic Ca^{2+} concentration, represented by the fura-2 fluorescence ratio (F_{340}/F_{380}), was measured *versus* time. Imaging data represent means ± S.E. with *x* averaged experiments, including *n* measured cells (*x*/*n*), and all other data represent means ± S.E. with *n* averaged experiments.

3*B* shows the corresponding current-voltage relationships (IVs) immediately after break-in. They revealed the typical features of wild-type TRPC4 currents with inward and outward rectification. Substitution of external TRPC channel-permeable monovalent cations by NMDG almost completely prevented the inward current, indicating that this current was carried by cations (see Fig. 3*A*). Fig. 3*C* shows the IVs during NMDG application in Fig. 3*A*. As a control, we transiently

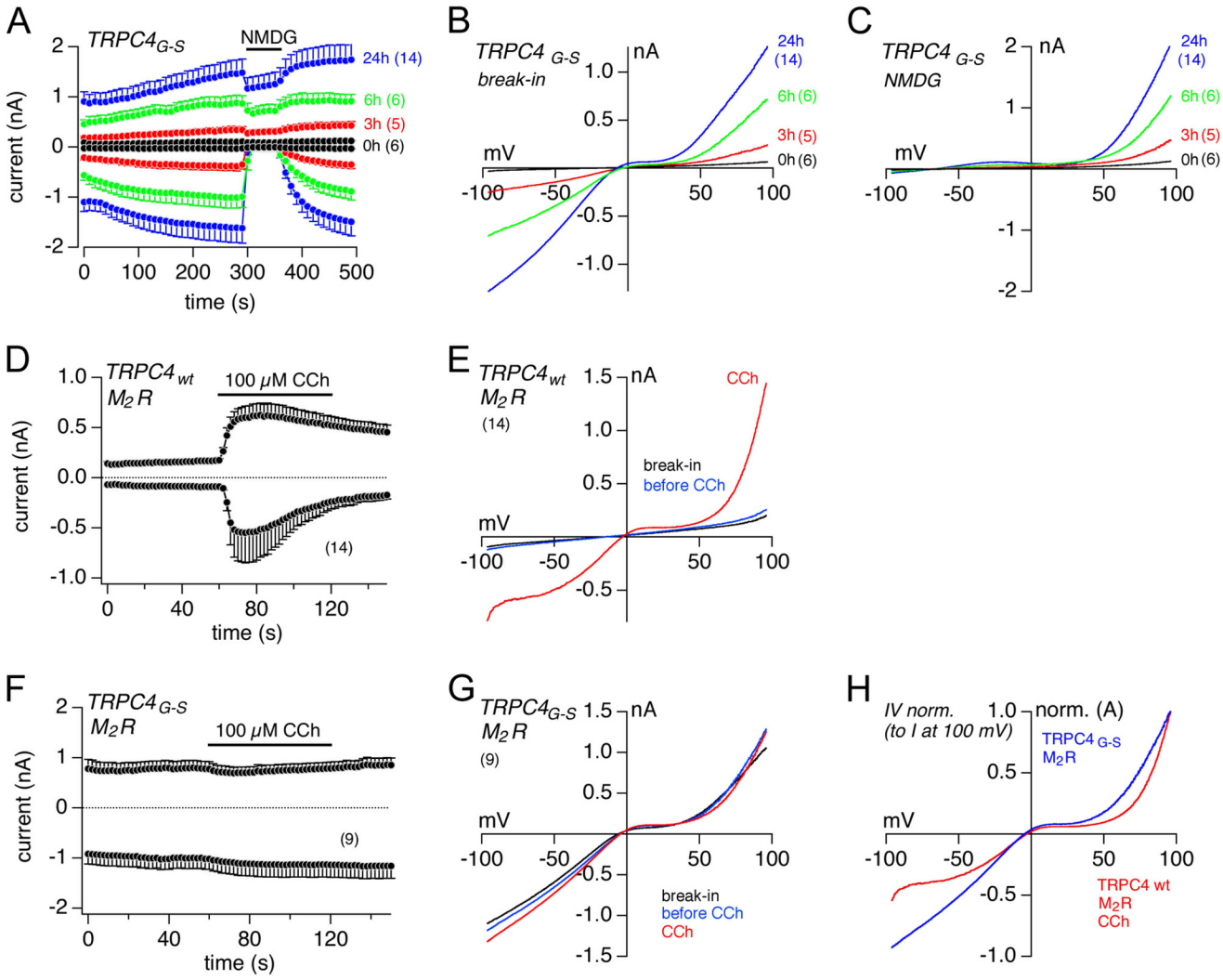

FIGURE 3. **TRPC4$_{G-S}$ cells reveal spontaneous cation-selective currents.** *A,* inward and outward currents at −80 and 80 mV, respectively, from HEK-293 cells inducibly expressing TRPC4$_{G-S}$ 0, 3, 6, and 24 h after induction plotted *versus* time. To verify cation conductance, NMDG-based solution was applied as indicated. The corresponding current-voltage relationships immediately after break-in and during the application of NMDG are displayed in *B* and *C*, respectively. *D,* current *versus* time in HEK-293 cells stably expressing the M_2R and transiently transfected with TRPC4$_{WT}$ for 24 h, challenged by the application of 100 μM CCh. *E,* IVs of currents in *D* immediately after break-in (*black*), before (*blue*), and during the application of CCh (*red*). *F,* currents at −80 and 80 mV from M_2R-expressing HEK-293 cells 24 h after transient expression of TRPC4$_{G-S}$ stimulated by 100 μM CCh at the indicated time. *G,* corresponding IVs immediately after break-in (*black*), before (*blue*), and during application of CCh (*red*). *H,* for comparison, normalized IVs (to I at 100 mV) from M_2R- plus TRPC4$_{G-S}$-expressing cells before application of CCh (*blue*; see *G*) and M_2R- plus TRPC4$_{WT}$-expressing cells during stimulation with CCh (*red*; see *E*). Data represent means ± S.E. with *n* averaged cells.

expressed TRPC4$_{WT}$ in a HEK-293 cell line stably expressing the M_2R and used the cells 24–48 h after transfection. These cells showed no basal activity but responded to application of 100 μM carbachol (CCh) with a large increase in current (Fig. 3*D*); the corresponding IVs at break-in, before and during CCh application, are shown in Fig. 3*E*. Transient expression (24 h) of TRPC4$_{G503S}$ into the same M_2R-expressing HEK-293 cells revealed spontaneous currents similar to 24 h after induction of the stable inducible TRPC4$_{G503S}$-expressing HEK-293 cells (Fig. 3*F*). Stimulation with CCh did not further increase the current. This suggests that the G503S mutation fully activates the TRPC4 channel. The corresponding IVs at break-in, immediately before and during CCh application, are shown in Fig. 3*G*. Fig. 3*H* shows the comparison of the normalized IVs of the TRPC4$_{WT}$ current activated by CCh and the spontaneous TRPC4$_{G503S}$ current obtained in the absence of CCh 24 h after transfection of the corresponding cDNA in M_2R-expressing HEK-293 cells.

After induction of protein expression, the TRPC5$_{G504S}$-expressing cells also revealed spontaneous outward and inward currents (Fig. 4*A*). Like the TRPC4$_{G503S}$ current, the TRPC5$_{G504S}$ current was reduced by substitution of permeable monovalent cations with NMDG in the bath solution (Fig. 4*A*). Fig. 4, *B* and *C,* shows the corresponding IV relationships immediately after break-in and in NMDG-based bath solution, respectively. Cells expressing wild-type TRPC5 did not show such a spontaneous current upon break-in using patch pipettes that contained 100 nM free Ca^{2+} (Fig. 4*D*). However, when they were dialyzed with 10 μM free Ca^{2+} via the patch pipette, an immediate Ca^{2+}-dependent activation of TRPC5 currents was obtained (Fig. 4, *D* and *E*). The TRPC5$_{G504S}$-expressing cells dialyzed intracellularly with 10 μM free Ca^{2+} did not reveal

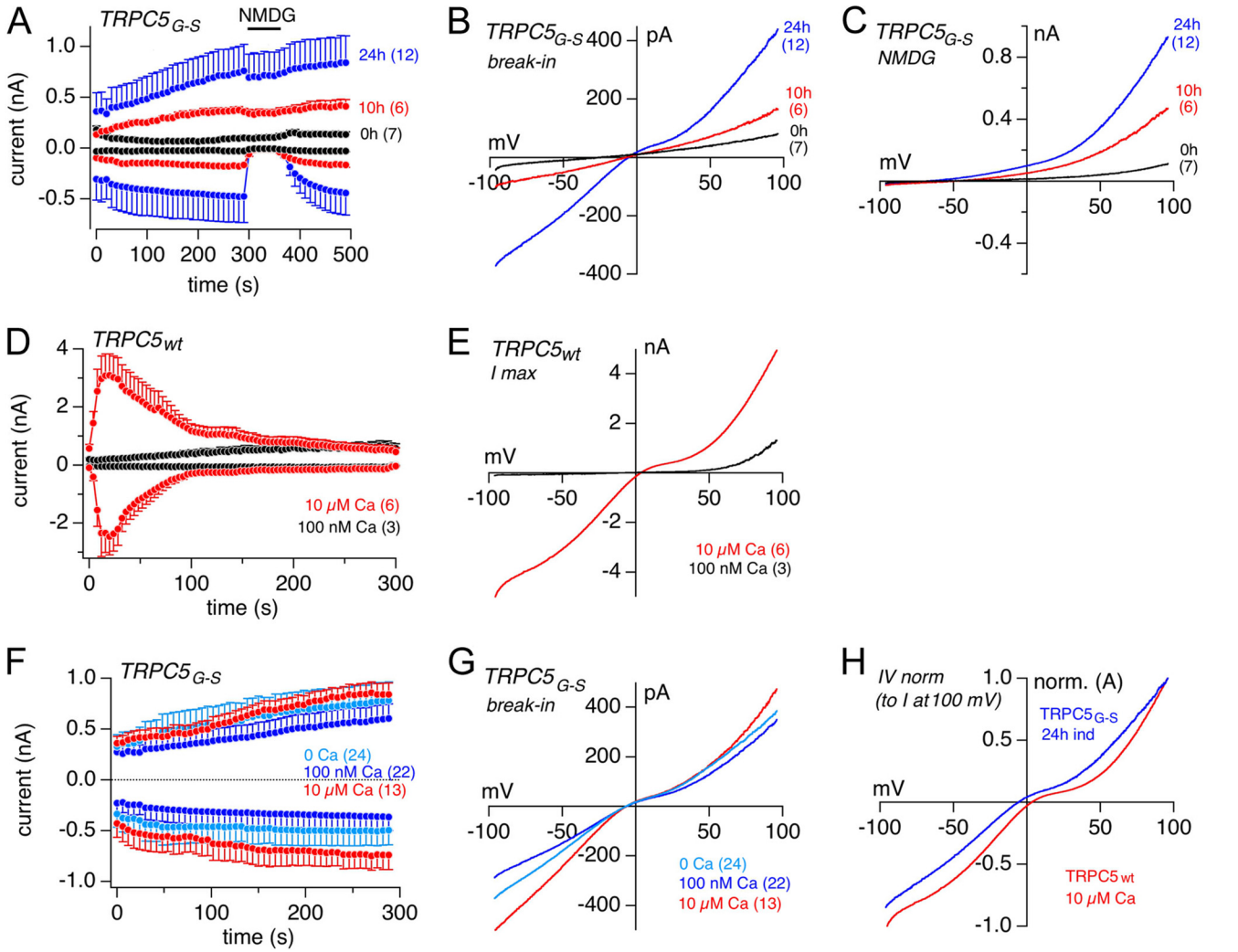

FIGURE 4. **TRPC5$_{G-S}$ cells reveal spontaneous cation-selective currents.** *A,* inward and outward currents at −80 and 80 mV, respectively, from HEK-293 cells inducibly expressing TRPC5$_{G-S}$ 0, 10, and 24 h after induction plotted *versus* time. To verify cation conductance, NMDG-based solution was applied as indicated. The corresponding current-voltage relationships (IVs) immediately after break-in and during the application of NMDG are displayed in *B* and *C*, respectively. *D,* current *versus* time in HEK-293 cells stably expressing TRPC5$_{WT}$, with the presence of 100 nM and 10 μM free Ca^{2+} in the patch pipette. *E,* IVs of maximal currents in *D* after break-in with 100 nM (*black*) and 10 μM free Ca^{2+} (*red*) in the patch pipette. *F,* currents at −80 and 80 mV from HEK-293 cells inducibly expressing TRPC5$_{G-S}$ 24 h after induction measured with 0 (*light blue*), 100 nM (*blue*), and 10 μM (*red*) free Ca^{2+} in the patch pipette plotted *versus* time. The corresponding IVs immediately after break-in are displayed in *G*. *H,* for comparison, normalized IVs (to I at 100 mV) from 24 h induced TRPC5$_{G-S}$ cells directly after break-in (*blue*; see *B*) and TRPC5$_{WT}$ cells activated by 10 μM free Ca^{2+} within the patch pipette (*red*; see *E*). Data represent means ± S.E. with *n* averaged cells.

such an immediate current increase on top of the constitutive activity (Fig. 4*F*). The average constitutive current amplitude in TRPC5$_{G504S}$-expressing cells was only slightly affected when cells were infused with 0, 100 nM, and 10 μM free Ca^{2+} (Fig. 4, *F* and *G*). Thus, as already seen for TRPC4$_{G503S}$, the G504S mutation in TRPC5 also seems to fully activate the current. Fig. 4*H* shows the comparison of the normalized IVs of the current activated in the presence of intracellular 10 μM free Ca^{2+} in TRPC5$_{WT}$ cells and the current from TRPC5$_{G504S}$ mutant cells 24 h after induction of TRPC5$_{G504S}$ protein expression.

Extracellular La^{3+} at 1–2 mM typically blocks all TRPC channels, but TRPC4 and TRPC5 are unique in that low extracellular concentrations of La^{3+} (100 μM) can potentiate already activated currents (21, 31). Therefore, we tested 2 mM and 100 μM extracellular La^{3+} to inhibit and potentiate, respectively, the constitutive TRPC4$_{G503S}$- and TRPC5$_{G504S}$-mediated currents. Both currents could be blocked by 2 mM extracellular La^{3+}, but none of them could be potentiated by 100 μM La^{3+} (Fig. 5, *A* and *D*). The IVs of TRPC4$_{G503S}$- and TRPC5$_{G504S}$-mediated currents at break-in, before and during high and low La^{3+} application, are shown in Fig. 5, *B* and *C*, and *E* and *F*, respectively.

Replacing Gly-503 in TRPC4 by Amino Acid Residues Other than Serine—With the G503S mutation, a nonpolar amino acid residue was replaced by a polar residue. We now replaced the glycine residue at position 503 in TRPC4 by the nonpolar amino acid residues methionine, leucine, and alanine. As already seen for G503S, the mutations G503M, G503L, and G503A all resulted in a constitutive TRPC4 activity, measured 24 h after transient transfection of the corresponding cDNA in HEK-293 M_2R cells (Fig. 6, *A–C*). Stimulation with CCh further increased the constitutive current of the TRPC4$_{G503L}$ and TRPC4$_{G503A}$ mutant channels (Fig. 6, *B* and *C*). The *upper graphs* in Fig. 6, *A–C,* show inward and outward currents at −80 and 80 mV,

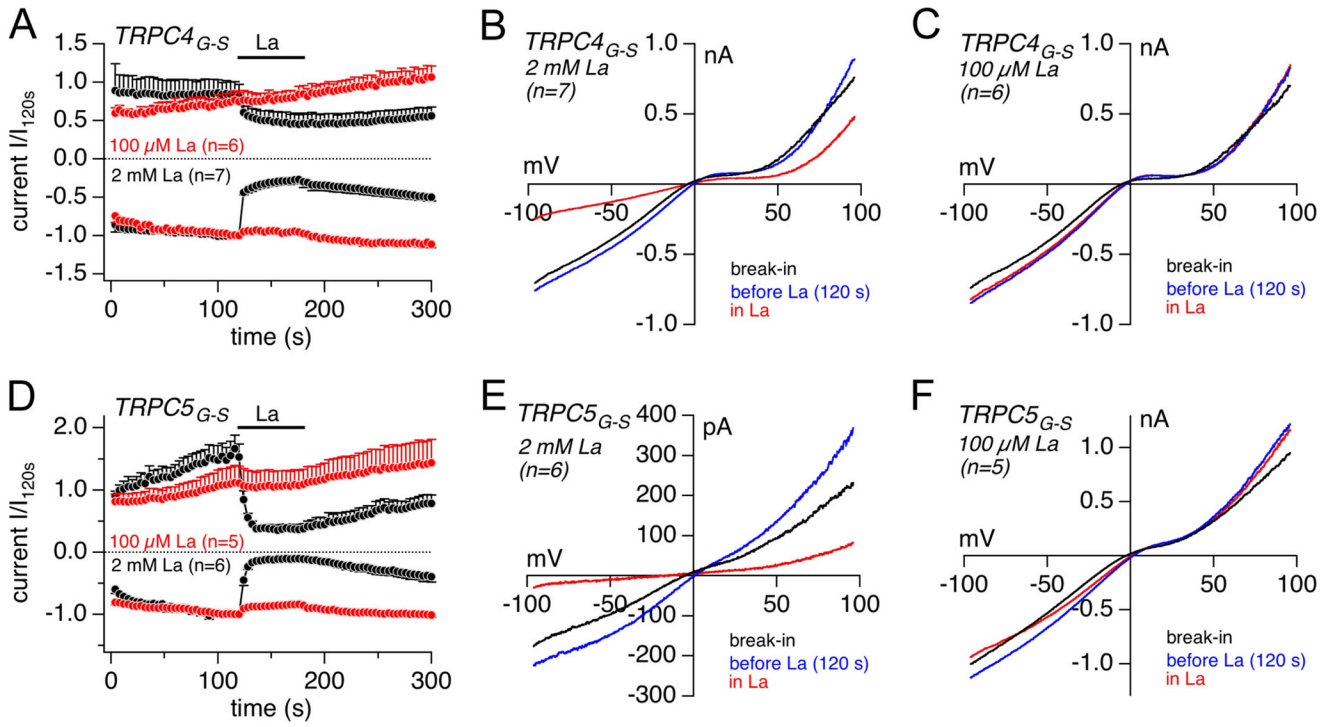

FIGURE 5. **Effects of external La^{3+} on $TRPC4_{G-S}$ and $TRPC5_{G-S}$ currents.** Normalized inward and outward currents at −80 and 80 mV, respectively, from HEK-293 cells inducibly expressing $TRPC4_{G-S}$ (*A*) and $TRPC5_{G-S}$ (*D*) 18–24 h after induction plotted *versus* time. As indicated by the *bars*, 100 μM (*red traces*) or 2 mM La^{3+} (*black traces*) were applied. Currents were normalized to the amplitude of the inward current at 120 s ($I/I_{120\,s}$) immediately before application of La^{3+}. The corresponding current-voltage relationships immediately after break-in (*black*), before (*blue*), and during the application of 2 mM (*B* and *E*) and 100 μM (*C* and *F*) La^{3+} (*red*) are displayed in *B* and *C* for $TRPC4_{G-S}$ and *E* and *F* for $TRPC5_{G-S}$, respectively. Data represent means ± S.E. with *n* averaged cells.

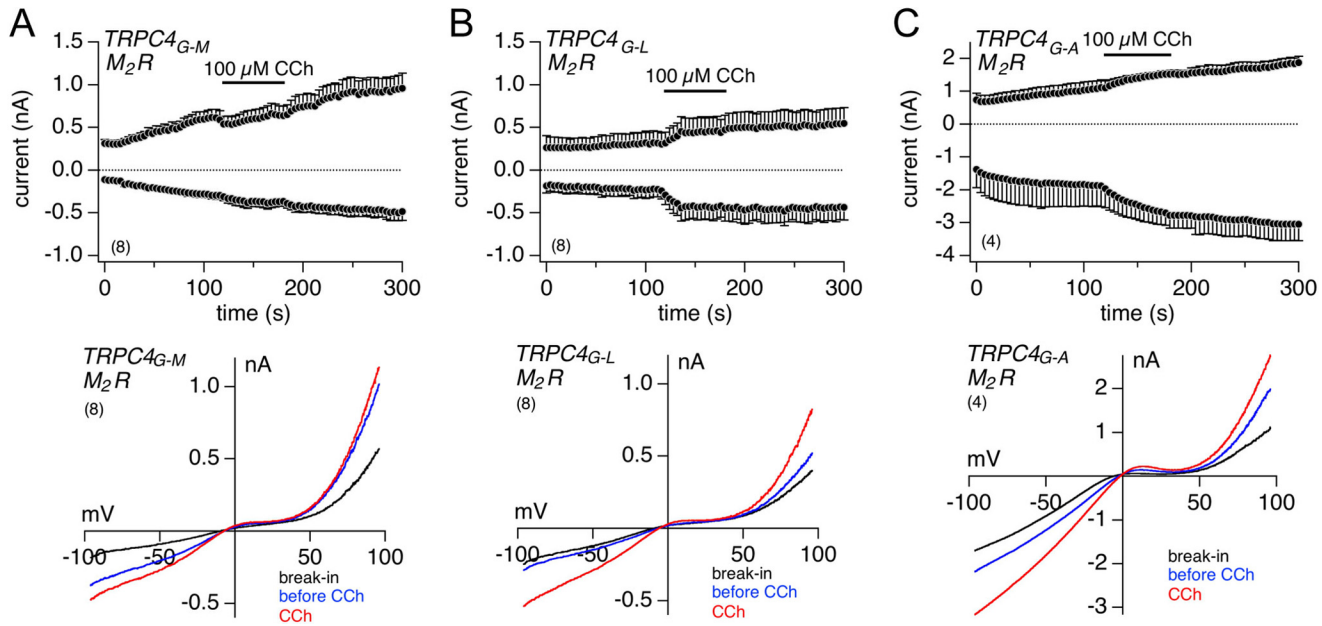

FIGURE 6. **Expression of additional TRPC4 mutations at Gly-503 in HEK-M_2R cells, and stimulation with carbachol.** *A–C,* inward and outward currents at −80 and 80 mV, respectively, from HEK-293 cells stably expressing the M_2 receptor and transiently expressing TRPC4 carrying single point mutations at Gly-503 (Gly-Met in *A*, Gly-Leu in *B*, and Gly-Ala in *C*) 24–48 h after transfection. *Bars* indicate the application of 100 μM carbachol. The corresponding current-voltage relationships immediately after break-in (*black*), before (*blue*), and during carbachol stimulation (*red*) are displayed below the time courses. Data represent means ± S.E. with n averaged experiments.

respectively, and the *lower graphs* display the IVs of the current at break-in (*black*) and before (*blue*) as well as during the application of CCh (*red*).

To determine the relative Ca^{2+} permeability of $TRPC4_{WT}$, $TRPC4_{G503S}$, and $TRPC4_{G503M}$, we measured the reversal potentials of currents from voltage ramps applied in 140 mM Na^+ (nominally Ca^{2+}-free, isoNa) and 125 mM Ca^{2+} (Na^+-free, isoCa) containing external solution (Fig. 7). Inward and outward currents at −80 and 80 mV, respectively, from HEK-293 cells stably expressing M_2R and $TRPC4_{WT}$ (activated by 100 μM

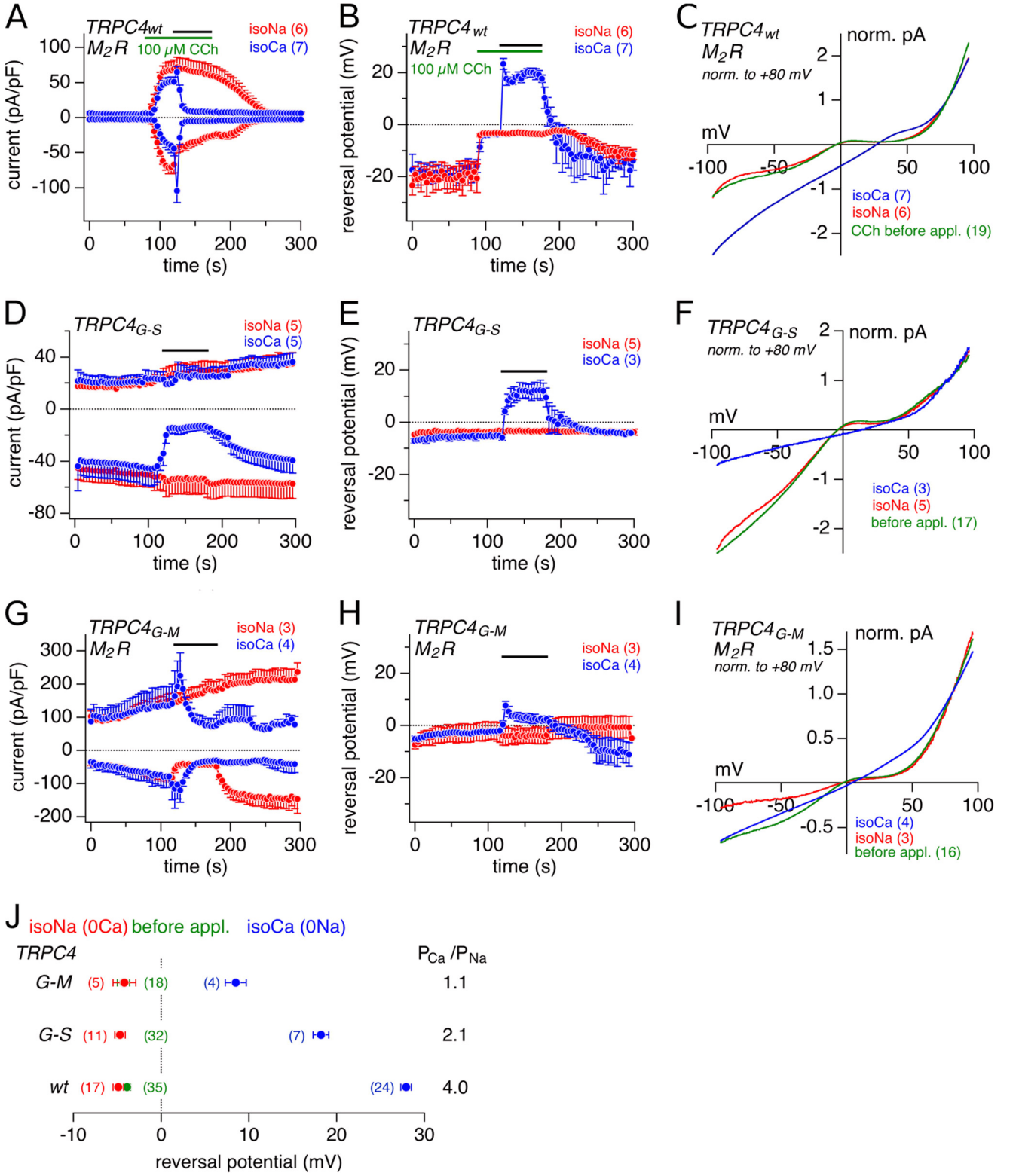

FIGURE 7. **Na^+ and Ca^{2+} permeability of $TRPC4_{WT}$, $TRPC4_{G-S}$, and $TRPC4_{G-M}$.** *A, D,* and *G,* inward and outward currents at −80 and 80 mV, respectively, from HEK-293 cells stably expressing M_2R and $TRPC4_{WT}$ (*A*), HEK-293 cells inducibly expressing $TRPC4_{G-S}$ 24 h after induction (*D*), and HEK-293 cells stably expressing M_2R and transiently 24–48 h $TRPC4_{G-M}$ (*G*). At the indicated time (*black bar*) isoNa (0Ca, *red*) or isoCa (0Na, *blue*) were applied onto the CCh-induced (*green bar*) TRPC4 current in *A*, and the constitutive active TRPC4 currents in *D* and *G*. *B, E,* and *H* represent the reversal potentials of the currents shown in *A*, *D*, and *G*, respectively. The corresponding TRPC4 current-voltage relationships (IVs) before (*green*) and in isoNa (*red*) and isoCa (*blue*) are shown in *C, F,* and *I*. All IVs were normalized to the amplitude of the outward current at 80 mV to compare the current-voltage relationship in dependence of the external cation conditions. *J,* summary of the reversal potentials of the currents via $TRPC4_{WT}$, $TRPC4_{G-S}$, and $TRPC4_{G-M}$ in control condition (before application, *green*, behind *red*), isoNa (0Ca, *red*), and isoCa (0Na, *blue*), and the calculated P_{Ca}/P_{Na}. The statistics include further experiments with application at different time points, which could not be averaged together with the traces shown above. Data represent means ± S.E. with *n* averaged experiments. *pA/pF*, picoampere/picofarad.

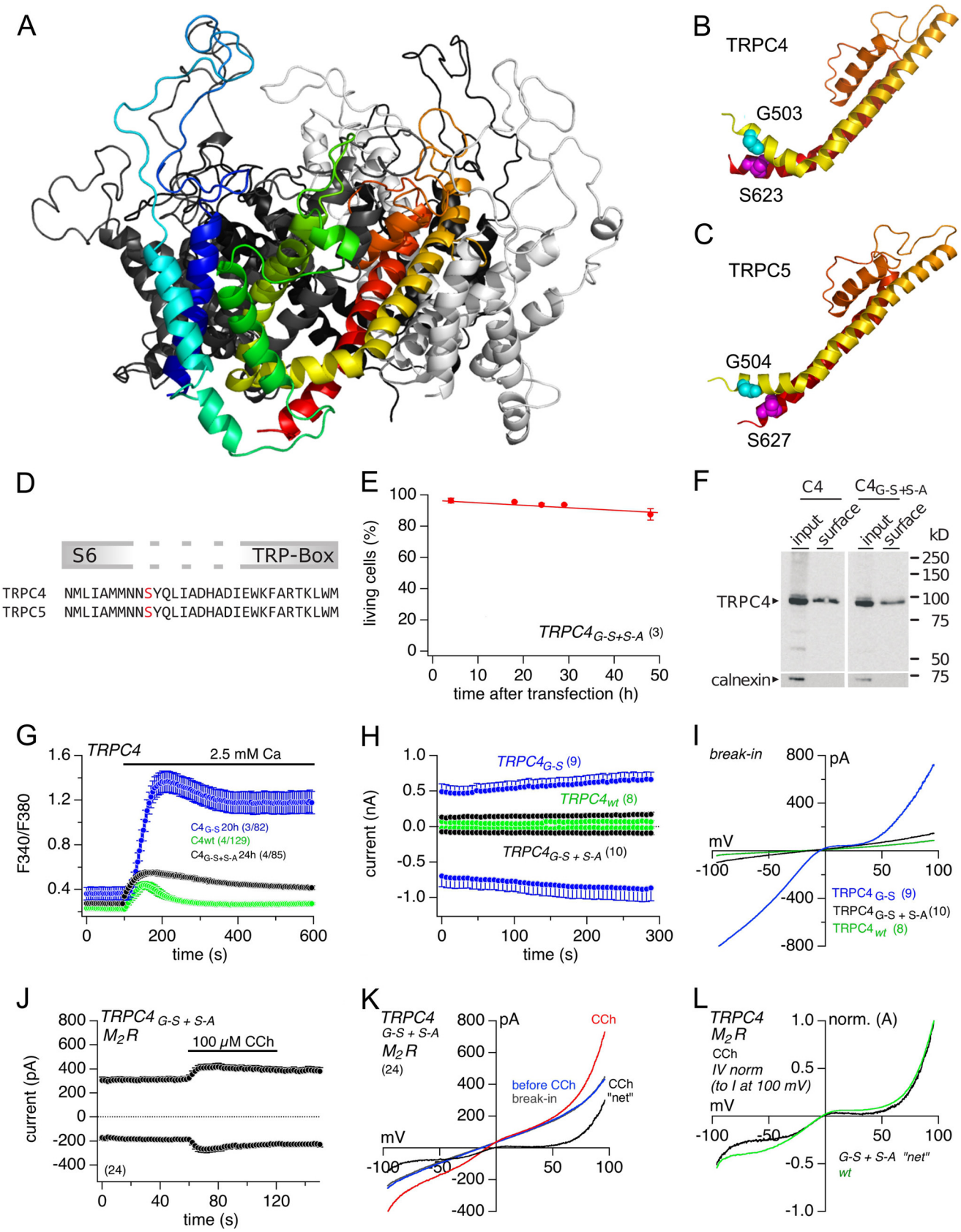
A
B
TRPC4
G503
S623
C
TRPC5
G504
S627
D
S6
TRP-Box
TRPC4 NMLIAMMNNSYQLIADHADIEWKFARTKLWM
TRPC5 NMLIAMMNNSYQLIADHADIEWKFARTKLWM
E
living cells (%)
TRPC4G-S+S-A (3)
time after transfection (h)
F
C4
C4G-S+S-A
input
surface
input
surface
kD
250
150
100
75
50
75
TRPC4
calnexin
G
TRPC4
2.5 mM Ca
F340/F380
C4G-S 20h (3/82)
C4wt (4/129)
C4G-S+S-A 24h (4/85)
time (s)
H
TRPC4G-S (9)
TRPC4wt (8)
TRPC4G-S + S-A (10)
current (nA)
time (s)
I
break-in
pA
mV
TRPC4 G-S (9)
TRPC4 G-S + S-A (10)
TRPC4 wt (8)
J
TRPC4 G-S + S-A
M2R
100 μM CCh
current (pA)
(24)
time (s)
K
TRPC4
G-S + S-A
M2R
(24)
pA
CCh
before CCh
break-in
CCh
"net"
mV
L
TRPC4
M2R
CCh
IV norm
(to I at 100 mV)
norm. (A)
mV
G-S + S-A "net"
wt

CCh), HEK-293 cells inducibly expressing $TRPC4_{G\text{-}S}$ 24 h after induction, and HEK-293 cells stably expressing M_2R and transiently 24–48 h $TRPC4_{G\text{-}M}$ are shown in Fig. 7, *A*, *D,* and *G*, respectively. Fig. 7, *B*, *E,* and *H* represent the reversal potentials of the currents shown in Fig. 7, *A*, *D,* and *G*, respectively. At the indicated time isoNa (*red*) or isoCa (*blue*) was applied. The corresponding TRPC4 current-voltage relationships, normalized to the amplitude of the outward current at 80 mV, before (*green*) and in isoNa (*red*) and isoCa (*blue*), are shown in Fig. 7, *C*, *F,* and *I*. Fig. 7*J* summarizes the reversal potentials of currents via $TRPC4_{WT}$, $TRPC4_{G503S}$, and $TRPC4_{G503M}$ under control conditions (before application, *green*), in the presence of isoNa (*red*) and isoCa (*blue*). Using Equation 1 (see "Experimental Procedures"), we calculated the relative Ca^{2+} permeability (P_{Ca}/P_{Na}) from the reversal potential shift in isoNa to isoCa solution as 4.0 for $TRPC4_{WT}$ (V_{rev}Na -4.9 ± 0.6 mV, $n = 17$; V_{rev}Ca 27.9 ± 0.6 mV, $n = 24$), 2.1 for $TRPC4_{G503S}$ (V_{rev}Na -4.7 ± 0.6 mV, $n = 11$; V_{rev}Ca 18.2 ± 0.9 mV, $n = 7$), and 1.1 for $TRPC4_{G\text{-}M}$ (V_{rev}Na -4.2 ± 1.3 mV, $n = 5$; V_{rev}Ca 8.5 ± 1.2 mV, $n = 4$).

Partial Rescue of the Wild-type Phenotype—Replacing the glycine residue at position 503 in TRPC4 by a polar (serine) or a nonpolar (methionine, leucine, and alanine) residue always led to constitutive activity. For the G503S and G504S mutations in TRPC4 and TRPC5, respectively, it is possible that the polar serine residue, which replaces the nonpolar glycine residue within the S4–S5 linker, interacts with another polar amino acid residue(s) within the channel proteins to keep the channel open. To find potential interaction partners, we constructed a homology model for TRPC4 on the basis of the known structure of a voltage-gated potassium (K_V) channel (Fig. 8*A*; one of the four subunits of TRPC4 is shown in color) (9). Fig. 8*B* shows the extracted structure for the sequence starting from linker S4–S5 via the transmembrane segment (TM) S5 (*yellow*), the pore region (*orange*) to the distal parts of TM S6 (*red*). According to the model, the S4–S5 linker contacts the distal end of the predicted TM S6 within the same subunit and potentially to helices S5 and S6 of neighboring subunits. In particular, the glycine 503 is located in about 8 Å distance from a serine residue at position 623 that was positioned in the model at the distal end of the predicted TM S6 of TRPC4. When the glycine at position 503 is replaced by a serine, a water-mediated contact may be formed between the hydroxyl groups of both amino acid residues or even a direct contact after some minor conformational rearrangements might occur. This interaction could elicit some constraint on the positions of the S4–S5 linker and the distal part of the S6, and as a result the channel may be forced into an open conformation. If such contacts were indeed formed, replacing the serine residue at position 623 by an alanine might counteract the impact of the mutant serine residue at position 503 in TRPC4 and yield a channel that can be regulated again. For comparison, we also generated a structural model for TRPC5 (Fig. 8*C*). This model also shows a similar proximity of the amino acids in the positions equivalent to TRPC4 Gly-503 and TRPC4 Ser-623, and the serine residue Ser-623 in TRPC4 is conserved in TRPC5 (Fig. 8*D*). Thus, we introduced a second mutation S623A into the $TRPC4_{G503S}$ mutant protein, expressed the double mutant in HEK-293 cells, and tested for cell survival, spontaneous Ca^{2+} influx, and ionic currents. Fig. 8*E* shows that the survival of HEK-293 cells was not affected by the expression of the double mutant $TRPC4_{G503S/S623A}$. The double mutated TRPC4 protein is expressed and present in the plasma membrane as shown by Western blot and surface biotinylation (Fig. 8*F*). In contrast to the spontaneous Ca^{2+} influx and ionic currents of the $TRPC4_{G503S}$-expressing HEK-293 cells, almost no constitutive Ca^{2+} influx (Fig. 8*G*) or currents (Fig. 8, *H* and *I*) appeared in cells expressing the double mutant. In this respect the double mutant closely resembles the wild-type TRPC4.

To activate $TRPC4_{G503S/S623A}$ channels, we expressed the $TRPC4_{G503S/S623A}$ mutant cDNA in the M_2R-expressing HEK-293 cells and applied 100 μM CCh. Fig. 8, *J* and *K,* shows the currents in $TRPC4_{G503S/S623A}$-expressing M_2R cells before and during the application of CCh. Stimulation with CCh significantly increased current size, and the normalized IV relationships of $TRPC4_{WT}$ and $TRPC4_{G503S/S623A}$ currents are almost identical (Fig. 8*L*). These data show that the $TRPC4_{G503S/S623A}$ protein is expressed in the plasma membrane and that $TRPC4_{G503S/S623A}$ channels, like $TRPC4_{WT}$ channels, are activated by CCh via muscarinic receptor activation. Apparently the introduction of a second mutation within the sequence distal to the S6 segment is offsetting the effect of the single G503S mutation introduced into the S4–S5 linker.

DISCUSSION

The data shown here support a TRPC4 and TRPC5 channel model in which the cytosolic S4–S5 linker is crucial for the

FIGURE 8. **Possible interaction between residues in S4–S5 linker and distal to S6 and partial reversion of the G503S-induced effect.** *A,* ribbon model of the murine TRPC4 tetramer structure based on the structure 3LUT of the Shaker potassium channel Kv1.2. The subunit in the front is shown in *color*, the other three subunits are shown in various *gray levels*. TM segments 1–4 are colored *blue* and *green*, TM segment S5 in *yellow*, the pore helix *orange*, and TM segment S6 in *red*. *B,* blow-up of the modeled conformation for one TRPC4 subunit encompassing the S4–S5 linker, the S5 TM domain (*yellow*), the pore helix (*orange*), and the S6 TM domain (*red*). Gly-503 at the N-terminal end of the S4–S5 linker is shown as *cyan spheres*; Ser-623 at the C-terminal end of the S6 helix is shown as *magenta spheres*. *C,* similar model as in *B* for murine TRPC5. *D,* alignment of the TRPC4 and TRPC5 amino acid sequences of the distal S6 segments and adjacent regions, including the TRP box. Serine residues 623 (TRPC4) and 627 (TRPC5) are indicated in *red*. *E,* viability assay of HEK-293 cells transiently expressing $TRPC4_{G\text{-}S/S\text{-}A}$ 0–48 h after transfection. The percentage of living cells, counted by a flow cytometer (Guava EasyCyte 8HT), was plotted *versus* time after transfection. *F,* Western blot and surface biotinylation. Surface expression of $TRPC4_{WT}$ and $TRPC4_{G\text{-}S/S\text{-}A}$ proteins 48 h after transfection of HEK-293 cells is shown. Calnexin was used as negative control for surface biotinylation. Fura-2 Ca^{2+} imaging (*G*) and currents at -80 and 80 mV (*H*) from cells transiently expressing $TRPC4_{G\text{-}S}$ and $TRPC4_{G\text{-}S/S\text{-}A}$ (24 h after transfection) or stably expressing $TRPC4_{WT}$. *I,* corresponding current-voltage relationships (IVs) immediately after break-in. *J,* currents at -80 and 80 mV from stable M_2R-expressing HEK-293 cells transiently expressing $TRPC4_{G\text{-}S/S\text{-}A}$ 24–48 h after transfection plotted *versus* time. CCh (100 μM) was applied as indicated by the *bar*. *K,* corresponding IVs of the current at break-in (*gray*, behind *blue IV*), before (*blue*), and during CCh application (*red*), and "net" CCh-induced current (current during CCh minus current before CCh; *black*). *L,* for comparison, normalized IVs (to I at 100 mV) from net CCh-induced currents in M_2R plus $TRPC4_{G\text{-}S/S\text{-}A}$-expressing cells (*black*; see *K*) or $TRPC4_{WT}$-expressing cells (*green*; normalized $TRPC4_{WT}$ IV is the same as already shown in Fig. 3*H*, *red IV*). Imaging data represent means ± S.E. with *x* averaged experiments, including *n* measured cells (*x*/*n*), and all other data represent means ± S.E. with *n* averaged cells.

regulation of channel gating. A single point mutation within this linker encodes hyperactive gain-of-function channels.

In the Shaker potassium channel, the S4–S5 linker forms a ring around the C-terminal end of the S6 helices and may trigger motion of the S6 helices to open or to close in response to voltage changes (10). A similar mechanism is likely to be conserved in TRPC channels, although TRPC proteins have no defined S4 voltage sensor, with only one charged residue within the predicted S4 amino acid sequence. The S4–S5 linker in TRPC4 and TRPC5 proteins resides within the cytosol and includes the sequence GPLQISLGRMLLD; the conservation of this motif is obvious within the members of the TRP proteins (see Fig. 1). In this study we have shown that replacing the conserved glycine residue at position 503 in TRPC4 by any other amino acid residue tested, polar (serine) or nonpolar (methionine, leucine, and alanine), leads to constitutive channel activity. This glycine residue seems to be invariant for keeping the TRPC4 channel, which is not receptor-activated, closed. All replacement amino acids form larger residues than glycine. Thus, maybe "simple" structural constraints might trigger motion of the S6 helices to open the channel pore similar to the mechanism of the voltage-gated potassium channel. Alternatively, it is possible that only the remarkable flexibility of the glycine peptide bond enables closure of the TRPC4 channel.

In the case of replacing the nonpolar glycine residue by the polar serine residue in TRPC4, constitutive activity could be reversed by a second mutation of a polar residue (serine) adjacent to the distal part of the S6 transmembrane domain, probably interacting with the serine in the S4–S5 linker via a water bridge, into a nonpolar residue (alanine). The double mutant $TRPC4_{G503S/S623A}$ channel was not constitutively open but could be stimulated by receptor activation. This suggests a possible mechanism of interaction of the S4–S5 linker with the distal S6 transmembrane domain to open the $TRPC4_{G503S}$ ion channel.

The Gly-to-Ser gain-of-function mutants in TRPC4 and TRPC5 are not further activated by the stimulation of G-protein-coupled signaling pathways via CCh and cytosolic high Ca^{2+}, respectively. Thus, the $TRPC4_{G503S}$ and $TRPC5_{G504S}$ gain-of-function mutations seem to fully open the channels. The corresponding IV relationships resemble the IV of wild-type channels maximally challenged by receptor activation (TRPC4) or high internal Ca^{2+} (TRPC5). Potentiation in the presence of 100 μM La^{3+} in the extracellular solution described for both TRPC4 and TRPC5 channels (21, 31, 32) did not occur for the mutant channels either. Both gain-of-function channels maintain robust steady-state inward and outward rectification indicating the existence of additional channel properties such as voltage dependence and intracellular Mg^{2+} block (33), which are hardly influenced by the mutation. However, the replacement of glycine 503 in TRPC4 changes the relative Ca^{2+} permeability from $P_{Ca}/P_{Na} = 4.0$ for WT to 2.1 for the Gly-to-Ser and 1.1 for the Gly-to-Met mutation. In the literature P_{Ca}/P_{Na} of TRPC4 varies from 1.1 for human TRPC4α (34) and mouse TRPC4β (35), and 7 for bovine TRPC4α (36).

Replacement of the conserved glycine at position 573 by a serine or a cysteine residue in the human, mouse, and rat TRPV3 proteins has been shown to be associated with the Olmsted Syndrome, a rare human congenital disorder, the spontaneous *Nh (non-hair)* mutation in mice, and *Ht (hypotrichosis)* mutation in rats (26–28). TRPV3 is expressed in keratinocytes, and the mutant channel proteins are associated with defective hair growth and dermatitis in the rodents and palmoplantar and periorificial keratoderma and severe itching in human patients. The mutant TRPV3 forms constitutively active channels (26, 29). In contrast, replacement of the corresponding glycine residue by a serine in TRPV1 ($TRPV1_{G563S}$) yields channels that exhibit only slightly enhanced basal activity (37).

However, plenty of other single point mutations in or close to the S4–S5 linker of TRP proteins are reported to result in constitutive channel activity and thus in diverse pathological phenotypes. For example, the T635A mutation in TRPC3 is associated with the loss of cerebellar Purkinje cells and the appearance of a so-called moonwalker phenotype as a result of cerebellar ataxia (30). The F550I mutation in the *Drosophila* TRP channel is associated with blindness and severe retinal degeneration (23). The human TRPV4 mutation R594H causes autosomal dominant spondylometaphyseal dysplasia, and the R616Q and V620I mutations cause brachyolmia (38). The A419P mutation in TRPML3 is causing a varitint-waddler phenotype with deafness and skin pigmentation defects in mice (39). The F380L mutation in the yeast yvc1 (yeast vacuolar conductance 1) causes stronger responses upon addition of osmotic shock-induced Ca^{2+} release from the vacuole into the cytosol (22, 40).

The mutant TRPC4 and TRPC5 channels described here cause cell death when expressed in HEK-293 cells, presumably because of the elevation of the intracellular Ca^{2+} concentration as well as membrane depolarization, as a result of constitutively active ion conductance. Growing the TRPC4 and TRPC5 mutant-expressing HEK-293 cells in the presence of SKF 96365, a nonspecific TRPC channel blocker, attenuates the cytotoxic phenotype. Lowering the Ca^{2+} concentration in the medium prevented cell death indicating that each mutant essentially contributes to Ca^{2+} influx rather than that other events downstream of TRPC4 and TRPC5 activation and/or expression are involved. Ca^{2+} imaging and whole-cell patch clamp experiments revealed that the mutated TRPC4 and TRPC5 channels are indeed constitutively active and lead to massive Ca^{2+} influx. The partial rescue by introducing a second mutation in TRPC4 adjacent to the distal part of the S6 transmembrane helix demonstrates that the Ca^{2+} influx and hence death of cells expressing the Gly-to-Ser mutant proteins are due to channel function.

Acknowledgments—We thank Karin Wolske, Heidi Löhr, and Christine Wesely for expert technical assistance.

REFERENCES

1. Gees, M., Colsoul, B., and Nilius, B. (2010) The role of transient receptor potential cation channels in Ca^{2+} signaling. *Cold Spring Harbor Perspect. Biol.* **2,** a003962
2. Wu, L. J., Sweet, T. B., and Clapham, D. E. (2010) International union of basic and clinical pharmacology. LXXVI. Current progress in the mammalian TRP ion channel family. *Pharmacol. Rev.* **62,** 381–404
3. Tsvilovskyy, V. V., Zholos, A. V., Aberle, T., Philipp, S. E., Dietrich, A.,

Zhu, M. X., Birnbaumer, L., Freichel, M., and Flockerzi, V. (2009) Deletion of TRPC4 and TRPC6 in mice impairs smooth muscle contraction and intestinal motility *in vivo*. *Gastroenterology* **137,** 1415–1424
4. Philipp, S., Hambrecht, J., Braslavski, L., Schroth, G., Freichel, M., Murakami, M., Cavalié, A., and Flockerzi, V. (1998) A novel capacitative calcium entry channel expressed in excitable cells. *EMBO J.* **17,** 4274–4282
5. Zimmermann, K., Lennerz, J. K., Hein, A., Link, A. S., Kaczmarek, J. S., Delling, M., Uysal, S., Pfeifer, J. D., Riccio, A., and Clapham, D. E. (2011) Transient receptor potential cation channel, subfamily C, member 5 (TRPC5) is a cold-transducer in the peripheral nervous system. *Proc. Natl. Acad. Sci. U.S.A.* **108,** 18114–18119
6. Gross, S. A., Guzmán, G. A., Wissenbach, U., Philipp, S. E., Zhu, M. X., Bruns, D., and Cavalié, A. (2009) TRPC5 is a Ca^{2+}-activated channel functionally coupled to Ca^{2+}-selective ion channels. *J. Biol. Chem.* **284,** 34423–34432
7. Kalia, J., and Swartz, K. J. (2013) Exploring structure-function relationships between TRP and Kv channels. *Sci. Rep.* **3,** 1523
8. Li, M., Yu, Y., and Yang, J. (2011) Structural biology of TRP channels. *Adv. Exp. Med. Biol.* **704,** 1–23
9. Long, S. B., Campbell, E. B., and Mackinnon, R. (2005) Voltage sensor of Kv1.2: structural basis of electromechanical coupling. *Science* **309,** 903–908
10. Long, S. B., Tao, X., Campbell, E. B., and MacKinnon, R. (2007) Atomic structure of a voltage-dependent K^+ channel in a lipid membrane-like environment. *Nature* **450,** 376–382
11. Labro, A. J., Boulet, I. R., Choveau, F. S., Mayeur, E., Bruyns, T., Loussouarn, G., Raes, A. L., and Snyders, D. J. (2011) The S4–S5 linker of KCNQ1 channels forms a structural scaffold with the S6 segment controlling gate closure. *J. Biol. Chem.* **286,** 717–725
12. Labro, A. J., Raes, A. L., Grottesi, A., Van Hoorick, D., Sansom, M. S., and Snyders, D. J. (2008) Kv channel gating requires a compatible S4–S5 linker and bottom part of S6, constrained by non-interacting residues. *J. Gen. Physiol.* **132,** 667–680
13. Grabe, M., Lai, H. C., Jain, M., Jan, Y. N., and Jan, L. Y. (2007) Structure prediction for the down state of a potassium channel voltage sensor. *Nature* **445,** 550–553
14. Prole, D. L., and Yellen, G. (2006) Reversal of HCN channel voltage dependence via bridging of the S4–S5 linker and Post-S6. *J. Gen. Physiol.* **128,** 273–282
15. Miller, M., Shi, J., Zhu, Y., Kustov, M., Tian, J. B., Stevens, A., Wu, M., Xu, J., Long, S., Yang, P., Zholos, A. V., Salovich, J. M., Weaver, C. D., Hopkins, C. R., Lindsley, C. W., McManus, O., Li, M., and Zhu, M. X. (2011) Identification of ML204, a novel potent antagonist that selectively modulates native TRPC4/C5 ion channels. *J. Biol. Chem.* **286,** 33436–33446
16. Bernsel, A., Viklund, H., Hennerdal, A., and Elofsson, A. (2009) TOPCONS: consensus prediction of membrane protein topology. *Nucleic Acids Res.* **37,** W465–W468
17. Chen, X., Wang, Q., Ni, F., and Ma, J. (2010) Structure of the full-length Shaker potassium channel Kv1.2 by normal-mode-based x-ray crystallographic refinement. *Proc. Natl. Acad. Sci. U.S.A.* **107,** 11352–11357
18. Larkin, M. A., Blackshields, G., Brown, N. P., Chenna, R., McGettigan, P. A., McWilliam, H., Valentin, F., Wallace, I. M., Wilm, A., Lopez, R., Thompson, J. D., Gibson, T. J., and Higgins, D. G. (2007) Clustal W and Clustal X. *Bioinformatics* **23,** 2947–2948
19. Waterhouse, A. M., Procter, J. B., Martin, D. M., Clamp, M., and Barton, G. J. (2009) Jalview Version 2–a multiple sequence alignment editor and analysis workbench. *Bioinformatics* **25,** 1189–1191
20. Eswar, N., Webb, B., Marti-Renom, M. A., Madhusudhan, M. S., Eramian, D., Shen, M. Y., Pieper, U., and Sali, A. (2006) Comparative protein structure modeling using Modeller. *Curr. Protoc. Bioinformatics,* Chapter 5, Unit 5.6
21. Jung, S., Mühle, A., Schaefer, M., Strotmann, R., Schultz, G., and Plant, T. D. (2003) Lanthanides potentiate TRPC5 currents by an action at extracellular sites close to the pore mouth. *J. Biol. Chem.* **278,** 3562–3571
22. Su, Z., Zhou, X., Haynes, W. J., Loukin, S. H., Anishkin, A., Saimi, Y., and Kung, C. (2007) Yeast gain-of-function mutations reveal structure-function relationships conserved among different subfamilies of transient receptor potential channels. *Proc. Natl. Acad. Sci. U.S.A.* **104,** 19607–19612
23. Hong, Y. S., Park, S., Geng, C., Baek, K., Bowman, J. D., Yoon, J., and Pak, W. L. (2002) Single amino acid change in the fifth transmembrane segment of the TRP Ca^{2+} channel causes massive degeneration of photoreceptors. *J. Biol. Chem.* **277,** 33884–33889
24. Krakow, D., Vriens, J., Camacho, N., Luong, P., Deixler, H., Funari, T. L., Bacino, C. A., Irons, M. B., Holm, I. A., Sadler, L., Okenfuss, E. B., Janssens, A., Voets, T., Rimoin, D. L., Lachman, R. S., Nilius, B., and Cohn, D. H. (2009) Mutations in the gene encoding the calcium-permeable ion channel TRPV4 produce spondylometaphyseal dysplasia, Kozlowski type, and metatropic dysplasia. *Am. J. Hum. Genet.* **84,** 307–315
25. Rock, M. J., Prenen, J., Funari, V. A., Funari, T. L., Merriman, B., Nelson, S. F., Lachman, R. S., Wilcox, W. R., Reyno, S., Quadrelli, R., Vaglio, A., Owsianik, G., Janssens, A., Voets, T., Ikegawa, S., Nagai, T., Rimoin, D. L., Nilius, B., and Cohn, D. H. (2008) Gain-of-function mutations in TRPV4 cause autosomal dominant brachyolmia. *Nat. Genet.* **40,** 999–1003
26. Lin, Z., Chen, Q., Lee, M., Cao, X., Zhang, J., Ma, D., Chen, L., Hu, X., Wang, H., Wang, X., Zhang, P., Liu, X., Guan, L., Tang, Y., Yang, H., Tu, P., Bu, D., Zhu, X., Wang, K., Li, R., and Yang, Y. (2012) Exome sequencing reveals mutations in TRPV3 as a cause of Olmsted syndrome. *Am. J. Hum. Genet.* **90,** 558–564
27. Lai-Cheong, J. E., Sethuraman, G., Ramam, M., Stone, K., Simpson, M. A., and McGrath, J. A. (2012) Recurrent heterozygous missense mutation, p.Gly573Ser, in the TRPV3 gene in an Indian boy with sporadic Olmsted syndrome. *Br. J. Dermatol.* **167,** 440–442
28. Asakawa, M., Yoshioka, T., Matsutani, T., Hikita, I., Suzuki, M., Oshima, I., Tsukahara, K., Arimura, A., Horikawa, T., Hirasawa, T., and Sakata, T. (2006) Association of a mutation in TRPV3 with defective hair growth in rodents. *J. Invest. Dermatol.* **126,** 2664–2672
29. Xiao, R., Tian, J., Tang, J., and Zhu, M. X. (2008) The TRPV3 mutation associated with the hairless phenotype in rodents is constitutively active. *Cell Calcium* **43,** 334–343
30. Becker, E. B., Oliver, P. L., Glitsch, M. D., Banks, G. T., Achilli, F., Hardy, A., Nolan, P. M., Fisher, E. M., and Davies, K. E. (2009) A point mutation in TRPC3 causes abnormal Purkinje cell development and cerebellar ataxia in moonwalker mice. *Proc. Natl. Acad. Sci. U.S.A.* **106,** 6706–6711
31. Schaefer, M., Plant, T. D., Stresow, N., Albrecht, N., and Schultz, G. (2002) Functional differences between TRPC4 splice variants. *J. Biol. Chem.* **277,** 3752–3759
32. Obukhov, A. G., and Nowycky, M. C. (2008) TRPC5 channels undergo changes in gating properties during the activation-deactivation cycle. *J. Cell. Physiol.* **216,** 162–171
33. Obukhov, A. G., and Nowycky, M. C. (2005) A cytosolic residue mediates Mg^{2+} block and regulates inward current amplitude of a transient receptor potential channel. *J. Neurosci.* **25,** 1234–1239
34. McKay, R. R., Szymeczek-Seay, C. L., Lievremont, J. P., Bird, G. S., Zitt, C., Jüngling, E., Lückhoff, A., and Putney, J. W., Jr. (2000) Cloning and expression of the human transient receptor potential 4 (TRP4) gene: localization and functional expression of human TRP4 and TRP3. *Biochem. J.* **351,** 735–746
35. Schaefer, M., Plant, T. D., Obukhov, A. G., Hofmann, T., Gudermann, T., and Schultz, G. (2000) Receptor-mediated regulation of the nonselective cation channels TRPC4 and TRPC5. *J. Biol. Chem.* **275,** 17517–17526
36. Philipp, S., Cavalié, A., Freichel, M., Wissenbach, U., Zimmer, S., Trost, C., Marquart, A., Murakami, M., and Flockerzi, V. (1996) A mammalian capacitative calcium entry channel homologous to *Drosophila* TRP and TRPL. *EMBO J.* **15,** 6166–6171
37. Boukalova, S., Marsakova, L., Teisinger, J., and Vlachova, V. (2010) Conserved residues within the putative S4–S5 region serve distinct functions among thermosensitive vanilloid transient receptor potential (TRPV) channels. *J. Biol. Chem.* **285,** 41455–41462
38. Verma, P., Kumar, A., and Goswami, C. (2010) TRPV4-mediated channelopathies. *Channels* **4,** 319–328
39. Grimm, C., Cuajungco, M. P., van Aken, A. F., Schnee, M., Jörs, S., Kros, C. J., Ricci, A. J., and Heller, S. (2007) A helix-breaking mutation in TRPML3 leads to constitutive activity underlying deafness in the varitint-waddler mouse. *Proc. Natl. Acad. Sci. U.S.A.* **104,** 19583–19588
40. Myers, B. R., Saimi, Y., Julius, D., and Kung, C. (2008) Multiple unbiased prospective screens identify TRP channels and their conserved gating elements. *J. Gen. Physiol.* **132,** 481–486